

SEISMIC ANALYSIS OF AN EMBEDDED RETAINING STRUCTURE IN COARSE-GRAINED SOILS

Luigi CALLISTO¹, Fabio M. SOCCODATO²

ABSTRACT

This paper presents the results of the dynamic numerical analysis of an ideal pair of cantilever retaining walls embedded in a coarse-grained soil. In the analysis, a hysteretic soil model was used, coupled with a perfectly plastic yield criterion. The retaining walls were designed using the pseudo-static approach with a small seismic coefficient, and their behaviour was checked under a more severe seismic input, consisting in a recorded acceleration history applied to the bedrock. Results are interpreted in detail, examining the evolution of the stress state in the soil, and evaluating the bending moments and the permanent displacements induced by the earthquake in the wall and in the soil. Results are also interpreted in terms of equivalent, pseudo-static seismic coefficients and the capability of a rigid-block Newmark analysis to reproduce the computed displacements is tested.

Keywords: Dynamic analysis, Excavations, Pseudo-static method, Retaining structures.

INTRODUCTION

The design of earth retaining structures under seismic conditions is often based on the pseudo-static Mononobe-Okabe (M.O.) theory, which was developed with reference to the limit equilibrium analysis of a rigid soil wedge. For an actual retaining structure subjected to seismic loading, the choice of the seismic coefficients to use in a pseudo-static approach is not straightforward. Moreover, when dealing with flexible embedded retaining structures, for which after excavation limit conditions may not have developed along the entire height of the wall, additional uncertainties do exist on the distribution of horizontal stresses along the retaining wall in both static and seismic conditions, which may affect the computed bending moments in the wall.

A better insight into the seismic behaviour of earth retaining structures can be obtained by performing dynamic analyses in which, with the aid of numerical methods, a reasonable approximation to the problem geometry is studied accounting for spatial and temporal variability of inertial forces during an earthquake. A key feature of the seismic behaviour of an earth retaining structure is that, under both static and seismic conditions, full mobilization of strength can be attained in soil zones interacting with the retaining wall. Therefore, on the one hand the soil model must provide a reasonable description of cyclic soil behaviour, and on the other hand it should allow for the development of plastic limit conditions. This is why a visco-elastic soil model, as used for instance by Veletsos & Younan (1997) and Degrande et al. (2002), which does not allow for the development of active and passive limit states, is not entirely satisfactory when studying the seismic behaviour of a real embedded retaining wall.

Most elastic-plastic constitutive models available in commercial numerical codes, which may be deemed acceptable for the static analysis of retained excavations, do not reproduce adequately cyclic soil behaviour. Specifically, along loading-unloading cycles of constant or decreasing amplitude, they

¹ Dipartimento di Ingegneria Strutturale e Geotecnica, Università di Roma 'La Sapienza', Email: luigi.callisto@uniroma1.it

² Dipartimento di Geoingegneria e Tecnologie Ambientali, Università di Cagliari

predict fully recoverable behaviour and therefore no hysteretic damping. Therefore, it is common to include in the formulation of the global dynamic equilibrium equations some numerical Rayleigh damping, in which the viscous damping matrix is a linear combination of the mass and stiffness matrices. However, the choice of the Rayleigh damping parameters is difficult and somewhat subjective, since the resulting damping ratio is strongly dependent on frequency and does not increase with strain.

MODEL DESCRIPTION

The analysis discussed in this paper was carried out using a different approach, in which no viscous damping was introduced, energy dissipation resulting entirely from the hysteretic soil behaviour. This was accomplished by describing cyclic soil behaviour through a hysteretic model available in the library of the Finite Difference code FLAC v.5 (Itasca, 2005). Basically, it consists in an extension to more general strain conditions of one-dimensional non-linear models that make use of the Masing (1926) rules. Under plane strain conditions, the relationship between shear stress τ and the corresponding shear strain γ may be expressed as:

$$\frac{\tau}{G_0} = \bar{\tau} = \frac{G_s(\gamma)}{G_0} \cdot \gamma = M_s(\gamma) \cdot \gamma \quad (1)$$

where $G_s(\gamma)$ is the secant shear modulus, function of γ ; G_0 is the small strain modulus; $\bar{\tau}$ and M_s are the normalised shear stress and shear modulus respectively. If the relationship between M_s and γ is known from an appropriate modulus decay curve, then the tangent normalised shear modulus M_t can be evaluated as:

$$M_t = \frac{d\tau}{d\gamma} = M_s + \gamma \frac{dM_s}{d\gamma} \quad (2)$$

and the tangent shear modulus can be computed as $G_t = M_t \cdot G_0$.

Strain reversal is detected by changes in sign of the dot product of the current strain increment and the direction of the previous mean strain path. Between strain reversals, the tangent shear modulus is evaluated from eq. (2), equating γ to the length of the strain path. At each strain reversal, the Masing rule is applied by scaling stress and strain differences by one half.

The analysis presented in this paper is relative to a pair of retaining walls embedded in an ideal coarse-grained soil. It was assumed that cyclic soil behaviour follows the relationship between normalised secant shear modulus M_s and γ shown in Figure 1(a) (Seed & Idriss 1970). This modulus decay curve can be approximated using the following 4-parameter sigmoidal expression for the function $M_s(\gamma)$:

$$M_s = y_0 + \frac{a}{1 + \exp(-(\log_{10} \gamma - x_0)/b)}, \quad (3)$$

using the values for the soil parameters a , b , x_0 and y_0 listed in Table 1. Figure 1(a) shows a comparison between the values of the damping ratio ξ predicted by the model for strain cycles of different amplitude and those provided by Seed & Idriss (1970) for coarse-grained soils. For $\gamma > 0.01$ %, the hysteretic model appears to over-predict the damping ratio. For $\gamma = 0.1$ %, which is a typical strain level attained during strong motion in the present seismic analysis, damping ratio is overpredicted by nearly 100 %. On the other hand, a comparison with the damping ratio curve published by Vucetic and Dobry (1991) for soils with a plasticity index $I_p = 0$, also shown in the figure, appears to be more satisfactory. It should be emphasised that, for a given modulus decay curve, the damping ratio is a result of the application of the Masing rules and it cannot be further

adjusted. Figure 1(a) shows for comparison the prediction of the hysteretic one-dimensional soil model available in the computer code NERA (Bardet & Tobita, 2001), which was calibrated on the same modulus decay curve. The resulting damping ratio curve is very similar to that predicted by the present model.

Figure 1(b) shows the stress-strain response of the FLAC hysteretic model to strain cycles of increasing amplitude ($\gamma_{\max} = 0.01, 0.02$ and 0.03%), obtained for $G_0 = 100$ MPa. It can be seen that the initial tangent to the backbone curve (τ vs. γ) is equal to G_0 , and that the tangent stiffness decreases with γ . The application of the Masing rules to the unloading-reloading paths produces hysteresis loops of increasing size.

Table 1. Values of parameters used for hysteretic damping (eq. 3).

parameter	a	b	x_0	y_0
value	0.9762	-0.4393	-1.285	0.03154

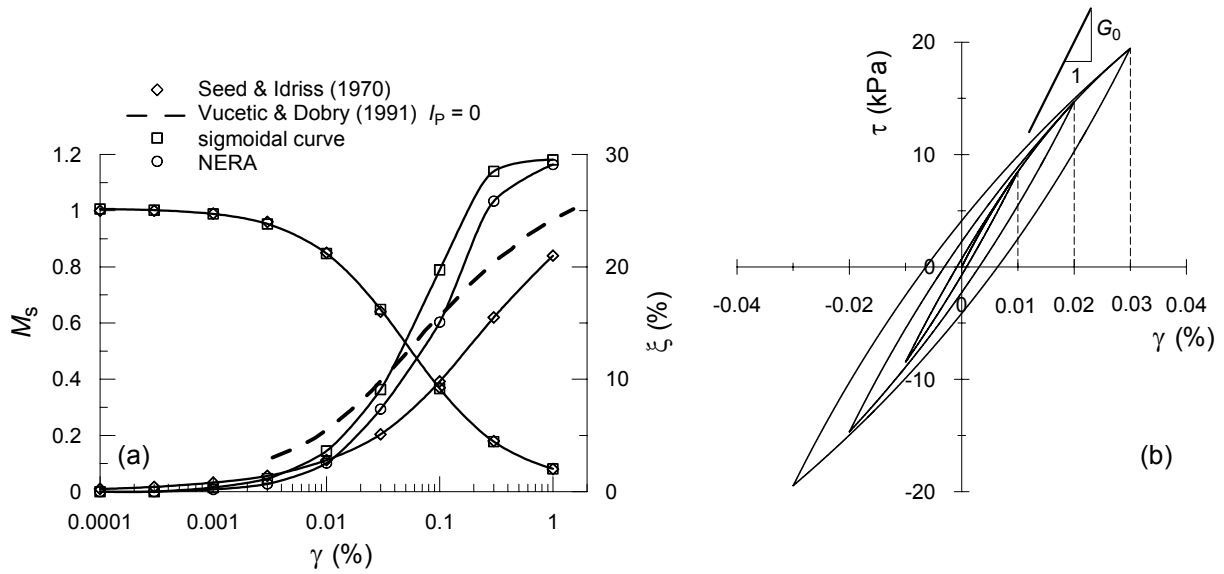


Figure 1. Modulus decay, damping ratio curves (a) and stress-strain response of the model (b).

NUMERICAL ANALYSIS

Figure 2 shows the finite difference grid, together with a schematic layout of the problem. An ideal excavation with a depth of 4 m is retained by a couple of embedded cantilevered retaining walls. The excavation is carried out in a dry coarse-grained soil with a constant angle of friction $\phi' = 35^\circ$, density $\rho = 2.04 \text{ Mg/m}^3$ and a stress-dependent small strain shear modulus $G_0 = 10000 \cdot p'^{0.5}$ (kPa), where p' is the mean effective stress. The bedrock is located at a depth of 30 m from the ground surface. The initial profiles of the shear wave velocity V_s and of the small strain shear modulus G_0 are shown in Figure 3(a,b).

A preliminary study of the dynamic response of the model was carried out in one-dimensional conditions (vertical propagation of SH waves). Initially, the dynamic input was made of single-frequency acceleration pulses (Ricker wavelets). Subsequently, a real seismic recording was used, selected from a database of Italian acceleration time histories recorded on rock. Specifically, the Tolmezzo NS time history was chosen, which is characterised by the highest Arias Intensity $I_a = 0.79 \text{ m/s}$ and by a peak acceleration $a_{\max} = 0.357 \text{ g}$. The accelerations were scaled to 0.35 g (which in the Italian code is the maximum acceleration on rock associated to a return period of 475 years) and

a low-pass filter at 15 Hz was applied for compatibility with the dimensions of the grid zones. The resulting time history has an Arias Intensity of 0.76 m/s.

Figure 3(c,d) shows the profiles of the maximum acceleration a_{\max} and the maximum shear strain γ_{\max} obtained from the one-dimensional analysis with the Tolmezzo recording. For comparison, results obtained with the linear equivalent approach (code EERA, Bardet et al., 2000) and with a different hysteretic model (code NERA) are also shown in the figure. Results obtained with the FLAC hysteretic model are quite similar to those obtained with the NERA hysteretic approach, particularly at small depths: they both show some amplification, the maximum acceleration at the ground level being 40 % larger than that applied to the bedrock. Conversely, the linear equivalent model (EERA) provides a somewhat different profile of maximum strains in the upper 15 m, and a peak ground acceleration about 70 % larger than the input at the bedrock.

For the present analysis, the hysteretic model described in the previous section was used to update at each calculation increment the shear modulus of an elastic-perfectly plastic soil model with a Mohr-Coulomb failure criterion and a non-associated flow rule (dilatancy angle $\psi = 0$). Therefore, during the analysis plastic strains associated to full strength mobilisation provided additional energy dissipation. The soil-wall contact was simulated using elastic-perfectly plastic interfaces with a friction angle $\delta = 20^\circ$. A small cohesion $c' = 0.5$ kPa was used to ensure numerical stability in the calculation.

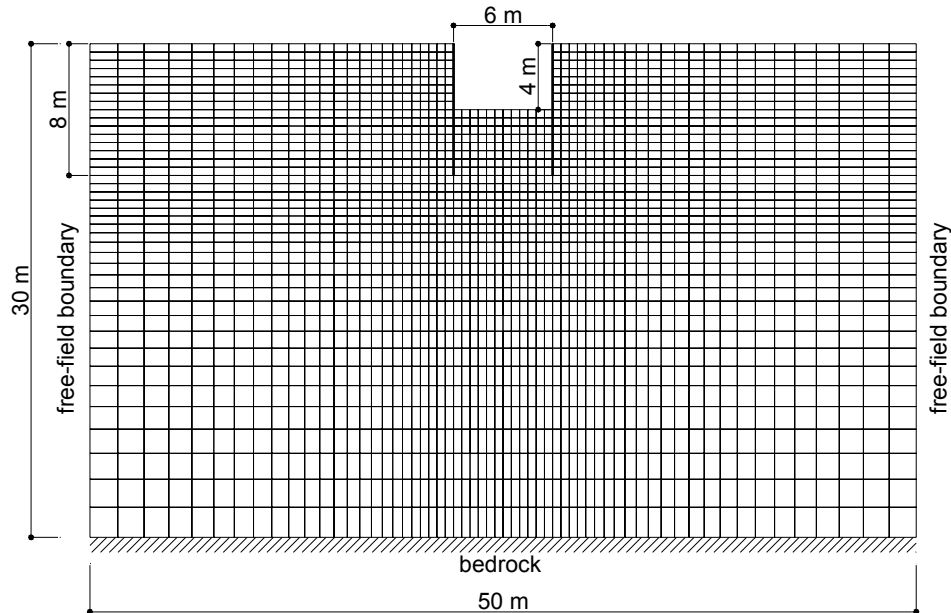


Figure 2. Problem layout and finite difference grid.

The embedded length of the walls, equal to 4 m, was computed through a pseudo-static limit equilibrium analysis, in which a horizontal seismic coefficient $k_h = 0.1$ was used and a global factor of safety equal to 1.8 was applied to the passive resistance. Active seismic forces were evaluated using the Mononobe-Okabe theory, while the passive ones were computed, assuming a soil-wall angle of friction equal to 20° , with the solutions developed by Chang (1981) based on an upper bound limit analysis. The pseudo-static method allowed to evaluate the distribution of the bending moments in the wall, which was designed accordingly. In the dynamic analysis, the retaining walls were simulated with elastic beam elements with axial and bending stiffness EA and EI corresponding to that of a bored-pile retaining wall with a diameter $D = 0.6$ m and a spacing $s = 0.7$ m. An additional analysis was carried out accounting for the development of plastic hinges in the retaining wall when bending moments attain the yielding value M_y . Table 2 reports the main input parameters for the analysis.

Zones in the finite difference grid of Figure 2 have a size of 0.5 m near the retaining wall and a maximum size of 1.8 m in the vicinity of the bedrock. The initial stress state was computed assuming

an earth pressure coefficient at rest $K_0 = 0.5$. Effects of the installation of the retaining walls were not modelled. The static analysis for the excavation was carried out in four steps, each time removing 1 m of soil. In this stage, a reduced shear modulus was used, equal to $0.3 G_0$, corresponding, on the modulus decay curve of Figure 1(a), to $\gamma \approx 0.1\%$. During the static stage, the grid was restrained horizontally and vertically at the base, while only horizontal displacements were prevented on the lateral sides.

The dynamic analysis was carried out applying the Tolmezzo acceleration time-history to the bedrock nodes. On the lateral sides, standard FLAC dynamic boundary conditions were applied: the grid was connected to “quite” boundaries (Lysmer & Kuhlemeyer, 1969) that in turn were connected to free-field boundaries, along which a free-field one-dimensional calculation was carried out in parallel with the main grid calculation. The time increment used in the explicit time integration scheme was $\Delta t = 6.25 \cdot 10^{-7}$ s.

Table 2. Input parameters for the analysis.

parameter	ρ (Mg/m ³)	c' (kPa)	ϕ' (°)	ψ	δ (°)	G_0 (kPa)	ν'	EA (kN/m)	EI (kNm ² /m)	M_y (kNm/m)
value	2.04	0.5	35	0	20	$10000 \cdot p^{0.5}$	0.2	$1.21 \cdot 10^7$	$2.72 \cdot 10^5$	150

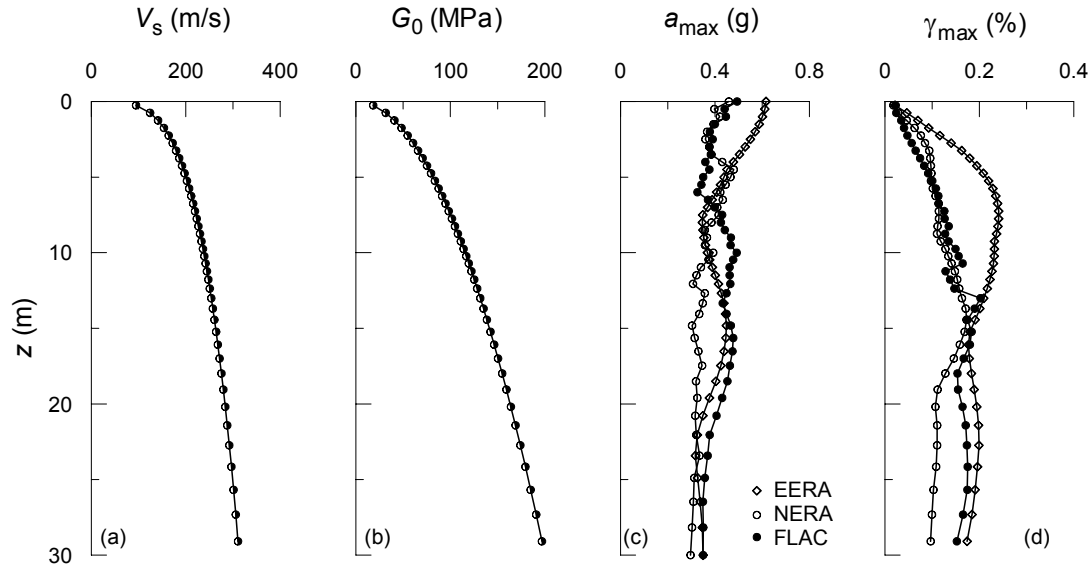


Figure 3. Profiles of V_s and G_0 (a,b), and results from one-dimensional analysis (c,d).

RESULTS

Amplification

Figure 4 shows the profiles of the maximum acceleration a_{max} along the free-field boundary (a), along soil zones behind the left wall (b) and along the centreline of the excavation (c), while Figure 5 shows some of the computed acceleration time histories and the corresponding Fourier amplitude spectra. After strong motion, the computed accelerations remain substantially higher than the input ones, showing that the earthquake energy is not completely dissipated by the hysteretic damping of the model. Also, both time histories and Fourier spectra show that high-frequency components of motion are generated in the calculation. While this result requires some deeper investigation, it is believed that it does not affect significantly the overall behaviour of the excavation, since, as it will be shown later, permanent displacements do not increase appreciably after $t = 8$ s.

The highest amplitudes for the input time history occur in the frequencies range of 2 to 4 Hz. Propagation through the soil results in a significant amplification in the frequency range of 1.0 to

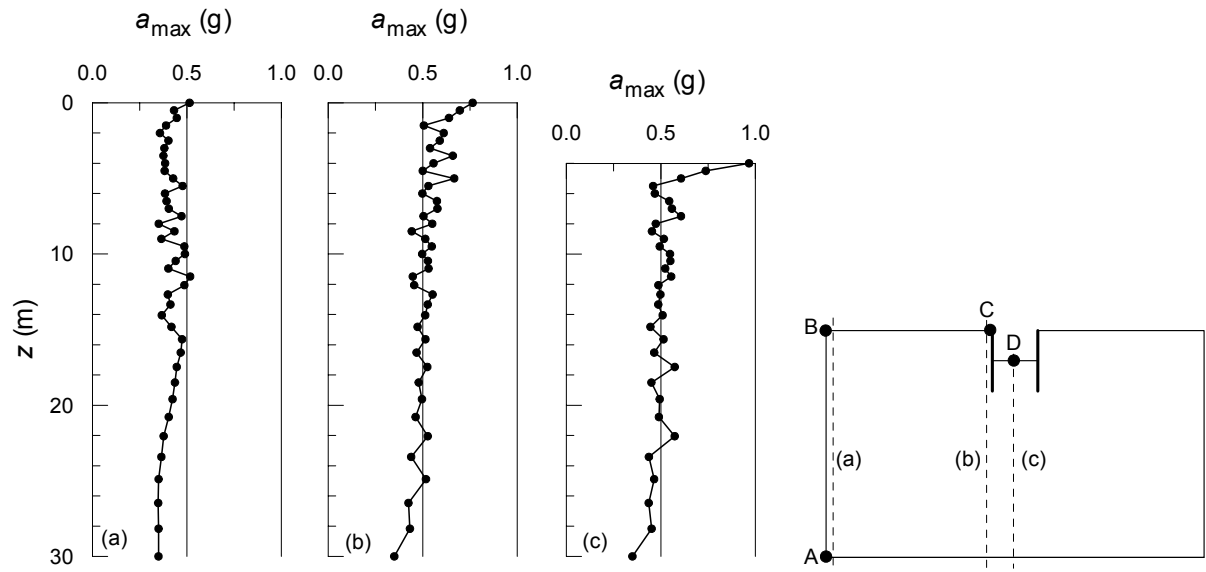


Figure 4. Profiles of maximum acceleration at different locations

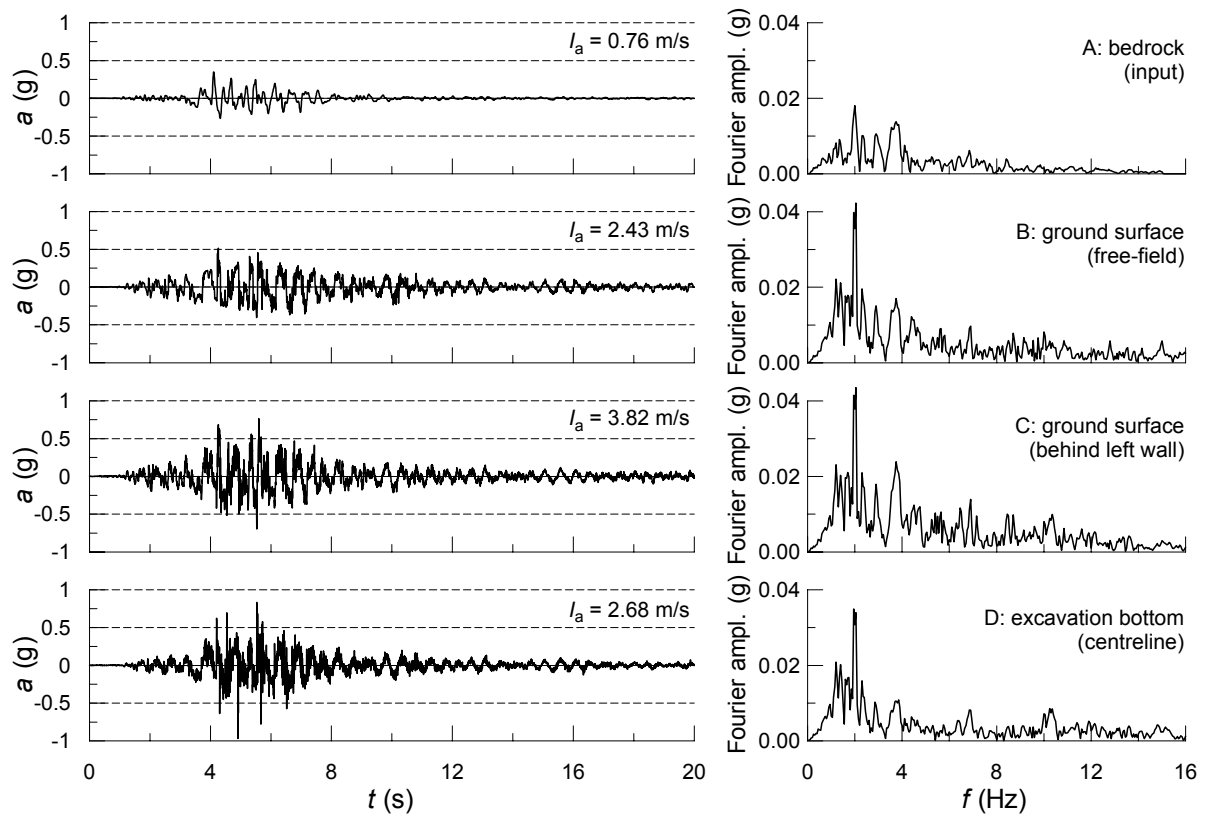


Figure 5. Computed acceleration time histories and Fourier spectra.

2.5 Hz. In the vicinity of the excavation, acceleration is amplified more than in the free-field, attaining the highest values at the ground level behind the wall and at the bottom of the excavation, where it reaches a value of 0.95 g. Inspection of the time histories shows that at the excavation bottom the peak acceleration is reached during a very small time interval, the worst time history being that computed behind the retaining wall. This observation is substantiated by the values of the Arias intensity I_a computed at 8 s, reported in Figure 5.

Stress state

Figure 6 shows the distribution of total horizontal stresses σ_h acting on the retaining walls, under static conditions (dashed line) and during the earthquake, after 5 and 20 s (lines with symbols). The figure also shows the theoretical distributions of σ_h for active and passive limit states, evaluated using the static active and passive earth coefficients K_a and K_p obtained by Lancellotta (2002) (solid lines). Under static conditions, active and passive limit states are fully mobilised down to $z = 4.5$ m. Below this depth, in front of the wall σ_h remains approximately constant, while behind the wall it increases up to the value at rest ($K_0 = 0.5$). This result is also visualised in Figure 7(a), that shows the contour plot of the mobilised strength, defined as the ratio τ/τ_{lim} between the maximum tangential stress acting at a point and the corresponding available strength.

Seismic shaking produces significant changes in the distribution of σ_h , which becomes non-symmetrical. Analysing the stress state at $t = 5$ s, it can be seen that σ_h increases both behind and in front of the left wall. This is consistent with changes in the ratio τ/τ_{lim} (Figure 7(b)), which decreases behind the wall and increases in front of the wall. At the selected time instant, the right wall shows a different behaviour: the active soil wedge almost reaches the toe and expands horizontally, its dimensions being compatible with an equivalent pseudo-static seismic coefficient $k_h = 0.35$. Therefore, active limit conditions are fully mobilised along most of the wall length, resulting in an overall decrease in σ_h . Consistently, in front of the right wall, a lower degree of strength mobilisation is computed, resulting in lower values of σ_h . In Figure 7(b) the slip surface for passive limit conditions in front of the left wall, predicted with the Chang (1981) method using $k_h = 0.35$, is also shown for comparison.

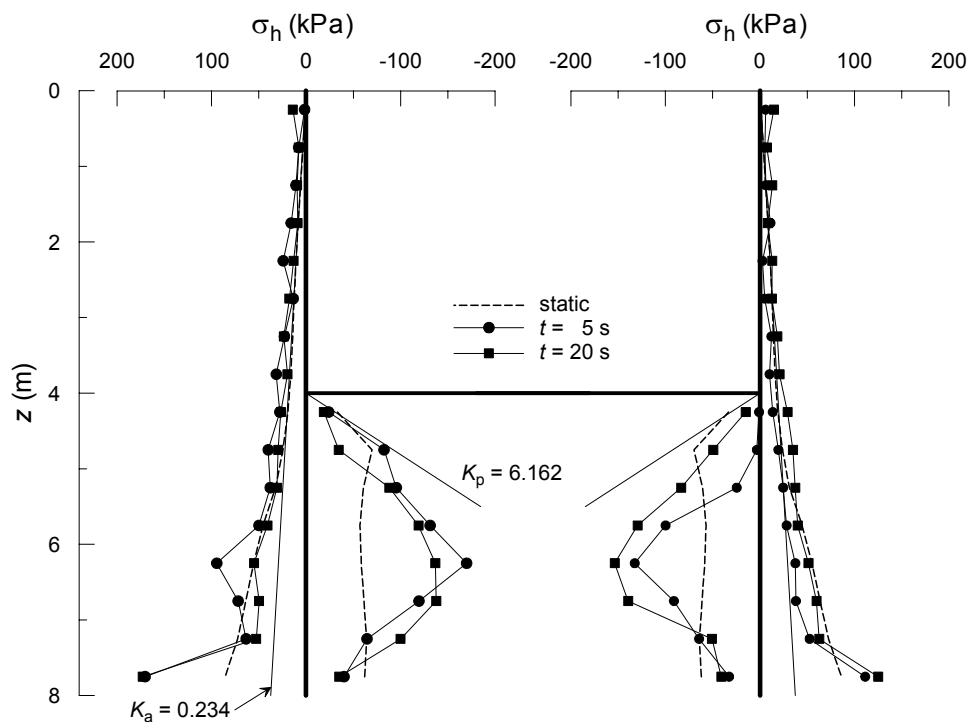


Figure 6. Computed horizontal stresses along the retaining walls.

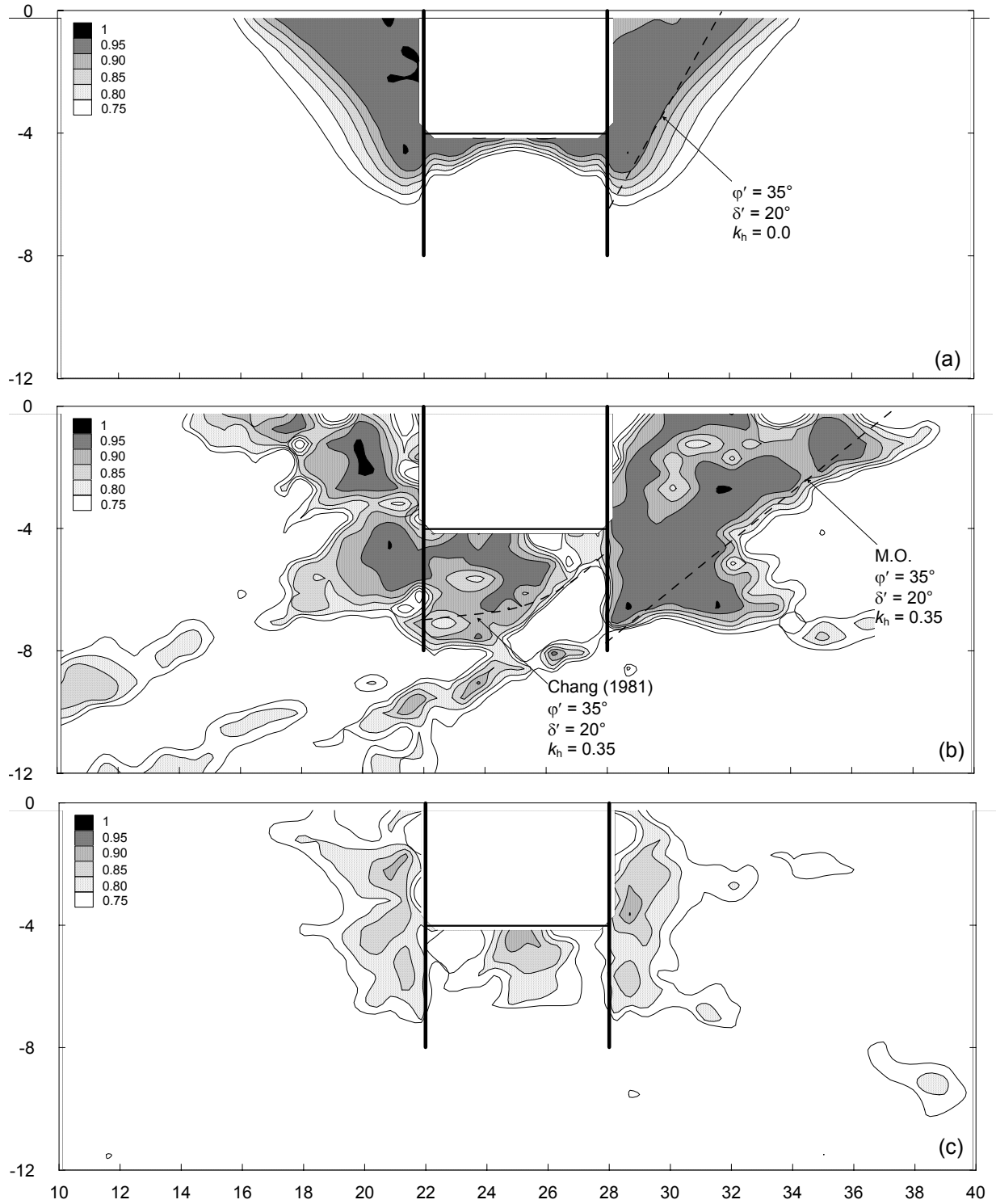


Figure 7. Contours of τ/τ_{lim} : (a) static; (b) $t = 5$ s; (c) $t = 20$ s.

At the end of the earthquake ($t = 20$ s), symmetry in the stress state is almost restored. Behind the walls, values of σ_h are somewhat larger than the corresponding initial ones and the stress state is more distant from active limit conditions (Figure 7(c)). The stress state in the soil immediately below the excavation bottom is no longer in a passive limit state. Between the walls, the area of maximum mobilised strength is deeper than in the initial conditions and the resulting distribution of horizontal stresses shows a maximum at a depth of about 2 m below the bottom of the excavation.

Bending moments

The distribution of the computed bending moments M in the retaining walls is shown in Figure 8 under static conditions, at $t = 5$ s and at $t = 20$ s. The figure also shows the envelopes of the maximum bending moments M_{\max} computed over the entire duration of the earthquake. As a result of a non-symmetrical acceleration time history, the distribution of M is not symmetrical, moments in the right wall being slightly larger. Seismic shaking produces a significant increment in the static bending moments and a downward shift of the position of the maximum moment.

At the end of the event ($t = 20$ s), the maximum bending moments locked in the retaining walls are still much higher than those computed under static conditions (by about 250 %). It can be seen that a reasonable approximation to the permanent values of M is obtained with a pseudo-static limit equilibrium analysis and a seismic coefficient $k_h = 0.16$. However, this satisfactory match is partly due to the overestimate of M under static conditions resulting from limit equilibrium analysis. This can also be inferred from the comparison between the computed static distribution of σ_h and those evaluated from limit equilibrium (Figure 6). A pseudo-static analysis shows that using $k_h = 0.16$ the global safety factor for the wall is still adequate, being about 1.56.

In design, it may not be necessary to make the retaining wall as strong as to absorb maximum bending moments: a wall designed to carry only the permanent values of M may suffice, provided that it is ductile enough to yield without a significant drop in strength. In Figure 8, a further distribution of M is shown, which was obtained assuming that the wall has a yield bending moment $M_y = 150$ kNm/m. In this case, the bending moments can never be higher than M_y , and this produces a small decrease in the permanent bending moments, associated to higher displacements as discussed in the following section.

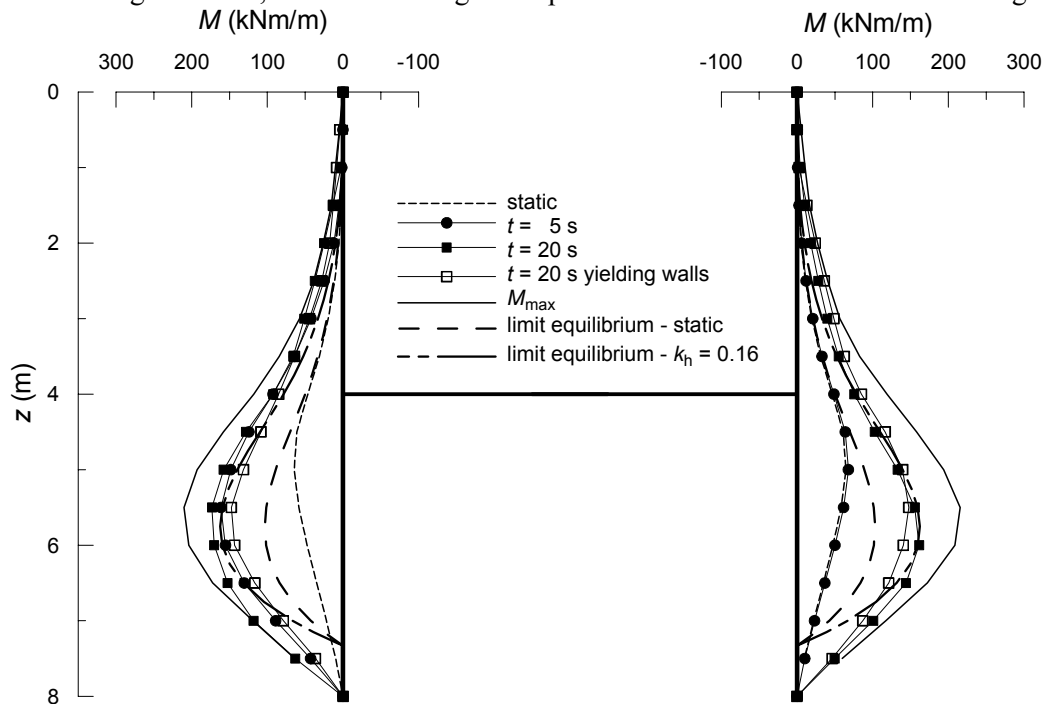


Figure 8. Computed bending moments in the retaining walls.

Displacements

Horizontal displacements u of the retaining walls, relative to the free-field lateral boundaries, are shown in Figure 9 under static conditions, at $t = 5$ s and at $t = 20$ s. During the earthquake, the walls move nearly as rigid bodies, rotating about a point close to the toe. This is consistent with the increase of σ_h behind the wall in the vicinity of their toe (Figure 6). The earthquake produces a substantial and permanent increase in the horizontal displacement of the walls. The maximum horizontal displacements for the left and the right walls are equal to about 0.04 m and 0.075 m respectively. It is interesting to observe that the displacement of the top relative to the toe is quite similar for both

retaining walls and is equal to about 0.06 m. Consistently, the vertical displacements w of the ground surface behind the walls are nearly symmetrical. They are plotted as a function of the distance from the right wall in Figure 9. A significant increase in the vertical displacements is produced by the earthquake, their maximum values being very close to the corresponding horizontal displacements of the top relative to the toe.

The analysis carried out with yielding walls produces larger horizontal and vertical displacements, as shown in Figure 9. The profiles of horizontal displacements show that a more significant curvature is generated by temporary yielding of the walls at different sections during the earthquake. Accordingly, vertical displacements are also larger and again their maximum value behind a wall is close to the horizontal displacement of the top relative to the toe.

Figure 10 shows the time histories for the horizontal displacements of the top of the walls relative to the toe and for the vertical settlements behind the walls. This plot shows only the displacements produced by the earthquake. Permanent displacements build up mainly between $t = 4$ s and $t = 8$ s remaining approximately stationary afterwards. The progressive accumulation of displacements suggests the possibility to use the Newmark method for evaluating the permanent displacements of the retaining walls. To this purpose, rigid-block calculations were carried out using the acceleration time histories computed at the ground surface behind both retaining walls, and finding the critical seismic coefficient k_c for which the rigid-block displacements match those computed in the dynamic analysis. The resulting values of k_c are equal to 0.19 and 0.17 for the left and the right wall respectively; the corresponding time histories of the permanent displacements are shown in Figure 10 with a bold line. However, under these seismic coefficients, the pseudo-static analysis predicts that the walls are not in a state of limit equilibrium: the available strength of the soil is not fully mobilised, the global factor of safety being $FS \approx 1.4$. Therefore, it appears that a rigid-block analysis is not capable to account for all the displacements computed in the dynamic analysis. This might be due to the interaction between the two walls, that may have reduced the strength available in the soil in front of the wall during seismic shaking. A parametric analysis investigating the effects of the wall spacing is deemed necessary to clarify this point.

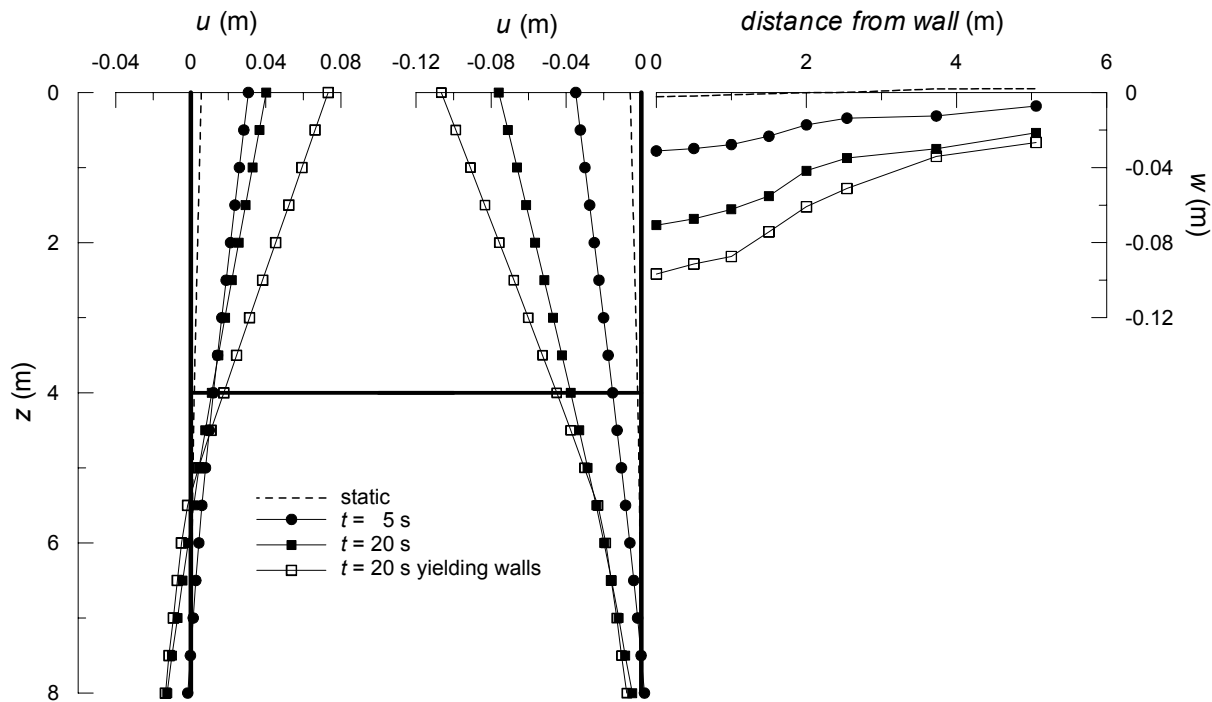


Figure 9. Computed displacements of walls and ground surface.

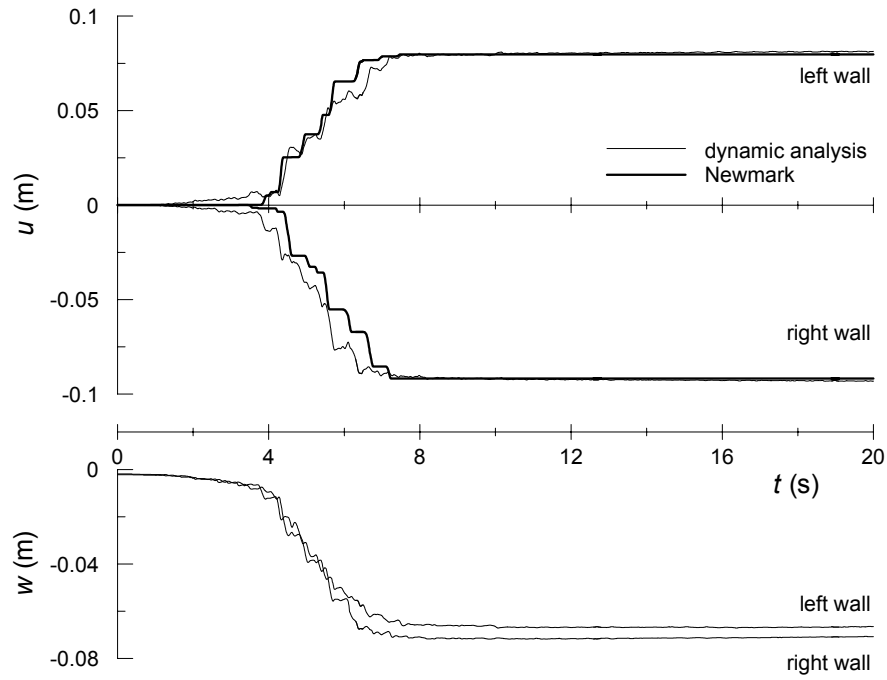


Figure 10. Time histories of horizontal (u) and vertical (w) displacements.

CONCLUSIONS

In this paper, the results of a dynamic analysis of a pair of cantilever retaining walls embedded in a coarse-grained soil was presented. A non-linear hysteretic soil model was used, coupled with a perfectly plastic yield criterion, in order to reproduce the main features of cyclic behaviour and the attainment of plastic limit states.

In a pseudo-static analysis of a flexible retaining wall, the seismic forces are assumed to be constant in space and time, and the seismic coefficient should be regarded as a conventional parameter that is supposed to describe synthetically the effects of the earthquake. The results discussed in this paper, relative to a particular case, showed that the interaction between the soil and the retaining wall is very complex, involving: different amplification of the motion amplitudes depending on the position relative to the excavation; redistribution of stresses on the retaining walls and in the soil interacting with the excavation; increase and redistribution of bending moments in the walls; and progressive accumulation of wall and soil displacements. Attempts to interpret some of these features in terms of the pseudo-static approach led to different values of the equivalent seismic coefficient k_h , depending on the particular aspect to reproduce.

Applying a seismic input to a problem characterised by geometrical symmetry produces a non-symmetric response. Therefore, in most cases it is necessary to include in the numerical model both walls supporting an excavation. In the present analysis, the spacing between the walls was equal to 1.5 times the embedded length and this may have produced a substantial interaction between the walls, different from that occurring under static conditions: significant strength mobilisation was computed in soil zones at a significant depth from the bottom, extending almost to the entire width of the excavation. This behaviour must be further explored carrying out additional analyses with different wall spacings.

ACKNOWLEDGEMENTS

The work presented in this paper is part of the *ReLUI*S research project, funded by the Italian Department of Civil Protection.

REFERENCES

- Bardet J. P. and Tobita T. "NERA. A computer program for Nonlinear Earthquake site Response Analyses of layered soil deposits". University of Southern California, Dept. of Civil Engineering. 2001.
- Bardet J., Ichii K. and Lin C. H. "EERA. A computer program for Equivalent-linear Earthquake site Response Analyses of layered soil deposits". University of Southern California, Dept. of Civil Engineering. 2000.
- Chang M.F. "Static and seismic lateral earth pressures on rigid retaining structures". Ph.D. Thesis, School of Civil Engineering, Purdue University, West Lafayette, IN. 1981.
- Degrade G., Praet E., Van Zegbroeck B. and Van Marcke P. "Dynamic interaction between the soil and an anchored sheet pile during seismic excitation". International Journal for Numerical and Analytical Methods in Geomechanics, vol. 26, 605-631. 2002.
- Itasca. "FLAC Fast Lagrangian Analysis of Continua" v. 5.0. User's Manual. 2005.
- Lancellotta R. "Analytical solution of passive earth pressure". Géotechnique, vol. 52, No. 8, 617-619. 2002.
- Lysmer, J., and Kuhlemeyer R.L. "Finite dynamic model for infinite media", Journal of Engineering Mechanics, Vol. 95(EM4), 859-877. 1969.
- Masing, G. "Eigenspannungen und Verfertigung bim Messing". Proceedings 2nd Int. Congress on Applied Mechanics, Zurich, 1926.
- Seed H.B. and Idriss I.M. "Soil moduli and damping factors for dynamic analysis". Report No. EERC 70-10, University of California, Berkeley, 1970.
- Veletsos A.S. and Younan A.H. "Dynamic response of cantilever retaining walls". Journal of Geotechnical and Geoenvironmental Engineering, ASCE, vol. 123, No. 2, 161-172. 1997.
- Vucetic M. and Dobry R. "Effect of soil plasticity on cyclic response". Journal of Geotechnical Engineering, ASCE, vol. 117, 89-107, 1991.